Title

Reprogramming the pancreatic cancer stroma and immune landscape by a silicasome nanocarrier delivering nintedanib, a protein tyrosine kinase inhibitor.

Authors

Luo, Lijia
Wang, Xiang
Liao, Yu-Pei
et al.

Publication Date

2024-02-01

DOI

10.1016/j.nantod.2023.102058

Peer reviewed

HHS Public Access

Author manuscript

Nano Today. Author manuscript; available in PMC 2025 February 01.

Published in final edited form as:

Nano Today. 2024 February ; 54: . doi:10.1016/j.nantod.2023.102058.

Reprogramming the pancreatic cancer stroma and immune landscape by a silicasome nanocarrier delivering nintedanib, a protein tyrosine kinase inhibitor

Lijia Luo[a,b], **Xiang Wang**[a,b], **Yu-Pei Liao**[a], **Xiao Xu**[a,b], **Chong Hyun Chang**[b], **Andre E. Nel**[a,b,*]

[a]Division of Nanomedicine, Department of Medicine, University of California, Los Angeles, CA 90095, USA

[b]California NanoSystems Institute, University of California, Los Angeles, CA 90095, USA

Abstract

The prevailing desmoplastic stroma and immunosuppressive microenvironment within pancreatic ductal adenocarcinoma (PDAC) pose substantial challenges to therapeutic intervention. Despite the potential of protein tyrosine kinase (PTK) inhibitors in mitigating the desmoplastic stromal response and enhancing the immune milieu, their efficacy is curtailed by suboptimal pharmacokinetics (PK) and insufficient tumor penetration. To surmount these hurdles, we have pioneered a novel strategy, employing lipid bilayer-coated mesoporous silica nanoparticles (termed "silicasomes") as a carrier for the delivery of Nintedanib. Nintedanib, a triple PTK inhibitor that targets vascular endothelial growth factor, platelet-derived growth factor and fibroblast growth factor receptors, was encapsulated in the pores of silicasomes via a remote loading mechanism for weak bases. This innovative approach not only enhanced pharmacokinetics and intratumor drug concentrations but also orchestrated a transformative shift in the desmoplastic and immune landscape in a robust orthotopic KRAS-mediated pancreatic carcinoma (KPC) model. Our results demonstrate attenuation of vascular density and collagen content through encapsulated Nintedanib treatment, concomitant with significant augmentation of the $CD8^+/FoxP3^+$ T-cell ratio. This remodeling was notably correlated with tumor regression in the KPC model. Strikingly, the synergy between encapsulated Nintedanib and anti-PD-1 immunotherapy further potentiated the antitumor effect. Both free and encapsulated Nintedanib induced a transcriptional upregulation of PD-L1 via the extracellular signal-regulated kinase (ERK) pathway. In summary, our pioneering approach involving the silicasome carrier not only improved antitumor angiogenesis but also profoundly reshaped the desmoplastic stromal and immune landscape within PDAC. These

*Corresponding author: Andre E. Nel, Division of Nanomedicine, Department of Medicine, University of California, Los Angeles, CA 90095, USA, ANel@mednet.ucla.edu.

CRediT authorship contribution statement:

Lijia Luo: Conceptualization, Experimentation, Data curation, Analysis, Writing – original draft. **Xiang Wang:** Animal experimentation. **Yu-Pei Liao:** Animal experimentation. **Xiao Xu:** Animal experimentation. **Chong Hyun Chang:** Nanoparticle physicochemical characterization. **Andre E. Nel:** Supervision, Principal investigator, Conceptualization, Writing – review & editing.

Declaration of Competing Interest

The authors declare the following competing financial interest(s): Andre E. Nel is co-founder and equity holder in Westwood Biosciences Inc. and Nammi Therapeutics. Nel also serves on the Board for Westwood Biosciences Inc. The remaining authors declare no conflict of interest.

Appendix A. Supplementary material

Supplementary data associated with this article can be found in the online version at doi:10.1016/j.nantod.2023.102058.

insights hold excellent promise for the development of innovative combinatorial strategies in PDAC therapy.

Graphical Abstract

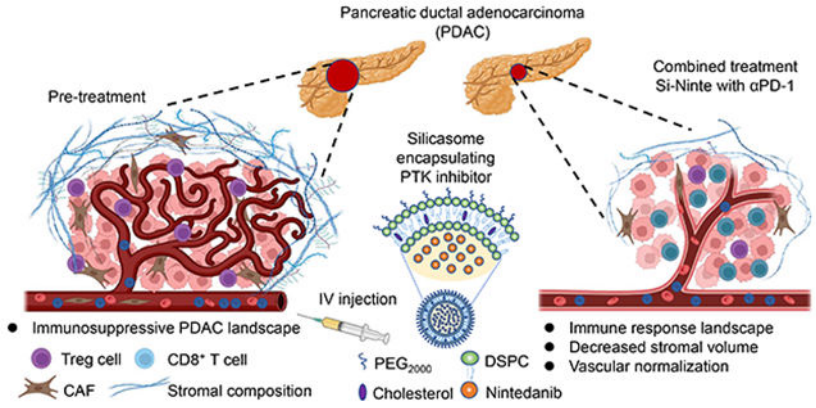

Keywords

PTK inhibitor; Drug delivery; Anti-angiogenesis; Pancreatic cancer; Tumor stroma; Immunotherapy

Introduction

Pancreatic ductal adenocarcinoma (PDAC) is the fourth leading cause of cancer-related deaths in the United States, with an alarming 5-year survival rate of only 12% [1]. Contributing to the high rates of mortality are shortcomings in surgery, chemotherapy, radiation therapy, and targeted therapies for PDAC patients who frequently present at an advanced disease stage with an aggressive tumor that display a formidable dysplastic stroma [2]. Not only does the presence of a robust extracellular matrix (ECM), cancer-associated fibroblasts (CAFs), and abnormal vasculature contribute to hindering therapeutic delivery, but also participate in generating an immune suppressive tumor microenvironment (TME) [3]. In an endeavor to improve PDAC treatment, several nanocarrier delivery systems have involved that offer advantages over traditional treatment approaches [4], [5], [6], [7],[8], [9]. Notable examples include liposome-encapsulated irinotecan (Onivyde) [8] and the albumin-paclitaxel nanocarrier (Abraxane) [9]. In addition, we have developed a silicasome platform, comprised of mesoporous silica nanoparticles (MSNPs) coated with a lipid bilayer, allowing improved drug loading capacity and the ability to ability to gain access to the PDAC site by a transcytosis mechanism [10]. The increased stability of the supported lipid bilayer and surface PEGylation contributes to stable drug retention in the circulation, culminating in improved pharmacokinetics (PK) and efficacy compared to liposome use for PDAC irinotecan delivery [11], [12], [13], [14].

In our ongoing quest to improve PDAC treatment, the role of protein tyrosine kinase (PTK) inhibitors has recently emerged as a new way for targeting the dysplastic PDAC tumor stroma, vascular permeability and boosting of the immune landscape

[15]. Specifically, PTK activity associated with the vascular endothelial growth factor (VEGF), platelet-derived growth factor (PDGF) and fibroblast growth factor (FGF) receptors are overexpressed in the PDAC TME, providing a target for kinase inhibitors [16], [17]. A particular promising candidate is the indolinone derivative, Nintedanib, emerging as a triple-PTK inhibitor, capable of interfering in the function of above growth factor receptors [18]. Nintedanib is also approved by the U.S. Food and Drug Administration (FDA) for the treatment of idiopathic pulmonary fibrosis and chronic fibrosing interstitial lung diseases [19], [20], [21]. Moreover, this drug has also been shown to exert immunomodulatory effects in preclinical colon, lung cancer and triple negative breast cancer models, predicting that it could be valuable in PDAC too [22]. However, in order to ensure that Nintedanib can effectively contribute to this class of cancer therapeutics, we need to consider that the limited water solubility of this complex organic molecule, known as (3Z)-3-[(4-{2-[(4-methylpiperazin-1-yl) methyl]-1H-benzimidazol-5-yl} pyrimidin-5-yl)amino]-3-(tetrahydro-2H-pyran-4-yl)propanoic acid, actually require processing in the gastrointestinal tract for its biodistribution in the lung [23]. We will delineate that this method of administration is not effective for accessing the dysplastic TME of PDAC, necessitating another mode of delivery.

Against this background, we set out to establish whether the medicinal chemistry properties of Nintedanib can be used for remote loading of a silicasome carrier, capable of improving the PK of drug delivery in a robust orthotopic model, which resembles human PDAC characteristics. We hypothesized that it would be possible to improve treatment efficacy through the drug effect on the tumor stroma, vasculature, and the immune landscape. We demonstrate that the weak basic properties of the PTK inhibitor could be used to achieve high drug loading capacity, with the silicasome achieving vascular trimming, reduction of collagen deposition, and improving the immune response at the PDAC site. Nintedanib also exerted unexpected transcriptional activation of the PD-L1 promotor, allowing immune response boosting in combination with an anti-PD1 monoclonal antibody. Taken together, these results demonstrate the promise of using PTK inhibitor therapy for targeting the PDAC stroma to improve drug delivery and immunotherapy.

Methods

Materials

1,2-distearoyl-sn-glycero-3-phosphocholine (DSPC), cholesterol (Chol) and 1,2-distearoyl-sn-glycero-3-phosphoethanolamine-N-[methoxy(polyethylene glycol)-2000] (ammonium salt) (DSPE-PEG2000) were obtained from Avanti Polar Lipids, USA. Nintedanib esylate, (2-Hydroxypropyl)-β-cyclodextrin (HP-β-CD) and IFN-γ were purchased from MedChem Express, USA. HEPES (4-(2-hydroxyethyl)-1-piperazineethanesulfonic acid), dextrose, EDTA-free protease inhibitor cocktail and RIPA lysis buffer were purchased from Sigma-Aldrich, USA. Dulbecco's modified Eagle medium (DMEM), penicillin, streptomycin and DiR dye ($DiIC_{18}(7)$ (1,1'-Dioctadecyl-3,3,3',3'-Tetramethylindotricarbocyanine Iodide) were purchased from Invitrogen. Fetal bovine serum (FBS) was purchased from Gemini Bio Products. PE anti-mouse CD274 (PD-L1) antibody was purchased from BD Biosciences, USA. Tris-Glycine SDS sample buffer, tris-glycine mini-protein gels (4-12%), ECL western

blotting substrate and West Pico PLUS chemiluminescent substrate were purchased from Thermo Fisher Scientific Inc., USA. 10x tris buffered saline (TBS), Tween 20, 10x tris/glycine/SDS, and 10x tris/glycine buffer were purchased from BIO-RAD, USA. Cell lysis buffer, phosphatase inhibitor cocktail, Vinculin (E1E9V) Rabbit mAb, phospho-p44/42 MAPK (Erk1/2) (Th202/Tyr204) Rabbit mAb, p44/42 MAPK (Erk1/2) Rabbit mAb, phospho-STAT3 (Tyr705) (D3A7) Rabbit mAb and STAT3 (124H6) Mouse mAb were purchased from Cell Signaling Technology, USA. Recombinant anti-PD-L1 antibody was purchased from Abcam, USA. *InVivo*MAb anti-mouse PD-1 (CD279) and *InVivo*Pure pH 7.0 Dilution Buffer were purchased from BioXCell, USA.

Synthesis and characterization of Silicasome-Nintedanib

Bare MSNPs and the trapping agent, triethylammonium sucrose octasulfate (TEA_8SOS), were prepared as we previously described [11], [12]. For silicasome synthesis, 50 mg of the lipid mix (DSPC/Chol/DSPE-PEG2000), in the molar ratio of 60:40:3, was dissolved in 0.1 mL pure ethanol at 65 °C. 1 mL of a preheated (65 °C) 80 mM TEA_8SOS, containing 40 mg MSNPs, was poured into the lipid mix, with stirring. After probe sonication with a 15/15 s on/off working cycle and a power output of 32.5 for 15 min, the solution was purified by size-exclusion chromatography, using elution of the Sepharose CL-4B column with a HEPES (5 mM HEPES, 5% dextrose, pH 6) to remove free TEA_8SOS.

For Nintedanib remote loading, 20 mg of Nintedanib was dissolved in 8 mL of HEPES-buffered dextrose (pH 6), before mixing and incubating with a TEA_8SOS soaked-in silicasome at 65 °C for 30 min. Following cooling on ice for 30 min, the obtained carrier was washed three times by centrifugation at 15,000 rpm. The drug carrier, designated Silicasome-Nintedanib (a.k.a. Si-Ninte), was subsequently suspended in a HEPES-buffered NaCl solution (4.05 mg/mL HEPES, 8.42 mg/mL NaCl, pH 7.2).

For the animal imaging studies, we also developed fluorescently labeled silicasomes by adding 0.2 mg $DiIC_{18}(7)$ (1,1'-Dioctadecyl-3,3,3',3'-Tetramethylindotricarbocyanine Iodide (DiR dye) into 50 mg of the lipid mix as described above. The rest of the synthesis procedure for Silicasome-Nintedanib-DiR abbreviated as Si-Ninte-DiR) was similar to Silicasome-Nintedanib.

Particle hydrodynamic size, size polydispersity index (PDI), and zeta potential were measured by a ZETAPALS instrument (Brookhaven Instruments Corporation). Nintedanib loading capacity was determined by calculating the weight ratio of Nintedanib relative to the total particle composition. The concentration of Nintedanib was determined by the UV-vis absorbance at 390 nm (M5e, Molecular Device, USA). MSNP mass was determined by TGA. Cryo-electron microscopy (CyroEM) micrographs were obtained in a TF20 FEI Tecnai-G2 instrument to demonstrate the the integrity and uniformity of the particles.

Cell culture

Kras-transformed murine pancreatic adenocarcinoma (KPC) cells, harvested from a spontaneous tumor originating from a transgenic KrasLSL-G12D/+; Trp53LSL-R172H/+; Pdx-1-Cre mouse model, were used for transduction with a luciferase-based lentiviral vector to derive KPC-luc cells, as previously described [11]. The KPC and KPC-luc cells were

cultured in DMEM with 10% (v/v) FBS, 100 units/mL of penicillin, and 100 mg/mL of streptomycin under 37 °C with 5% CO_2.

Flow cytometry

For assessment of PD-L1 expression, KPC cells were seeded in 24-well plates at a density of 5×10^4 cells per well for 24 h, before the addition of fresh medium containing PBS, free Nintedanib or Si-Ninte, with or without IFN-γ, for a further 24 h. The concentration of Nintedanib was 0.5 or 1 μM, and that of IFN-γ was 10 ng/mL. Nintedanib esylate was dissolved in DMSO before further dilution. KPC cells were washed with cell staining buffer, before staining with PE-conjugated anti-PD-L1 on ice, according to the manufacturer's instructions. The assessment of PD-L1 expression was evaluated in a LSRFortessa flow cytometer (BD Biosciences) and analyzed using FlowJo software.

Western blotting

Protein extraction and performance of Western blotting followed conventional protocols. To prepare protein extraction, KPC cells were seeded in 6-well plates at a density of 4×10^5 cells per well for 24 h, before incubation with PBS, free Nintedanib or Si-Ninte for a further 24 h. The Nintedanib concentration was 1 μM. After placing the plate on ice and washing the cells with PBS, ice-old RIPA lysis buffer, containing an EDTA-free protease inhibitor cocktail and phosphatase inhibitor cocktail, was added. Following scraping adherent cells, the suspension was transferred into a pre-cooled microcentrifuge tube and kept at 4°C for 30 min before centrifugation at 12,000 rpm for 20 min. The supernatants were placed in a fresh tube, following the determination of protein concentration for each cell lysate by a BCA assay.

To prepare tissue protein extraction, frozen tumor samples were mechanically disrupted into small pieces with clean pre-cooled tools on ice, and thoroughly homogenized in ice-cold RIPA lysis buffer containing the protease inhibitor and phosphatase inhibitor cocktail cocktails, using a mechanical tissue homogenizer. The lysed suspension was kept at 4°C for 2 h before centrifugation at 12,000 rpm for 20 min. The supernatants were collected into a fresh tube before the determination of protein concentration. Equal amounts of protein from cell and tumor specimens were loaded in tris-glycine mini-protein gels (4-12%) for electrophoresis. After transferring the proteins onto nitrocellulose membrane overnight at 4 °C, these were blocked for 1 h at room temperature with 5% milk in tris buffered saline containing 0.1% Tween 20 (TBST). Following 3 times washing by TBST, membranes were incubated overnight at 4 °C with an anti-Vinculin Rabbit mAb, diluted 1:1000, Phospho-p44/42 MAPK (Erk1/2) Rabbit mAb, diluted 1:1000, p44/42 MAPK (Erk1/2) Rabbit mAb, diluted 1:1000, Phospho-STAT3 Rabbit mAb, diluted 1:2500, or STAT3 Mouse mAb, diluted 1:5000. Membranes were washed and incubated with an anti-rabbit IgG HP-linked antibody (dilution 1: 1000 or 1: 2500) for 1 h at room temperature. After 3 washes, antigen-antibody reaction was detected using ECL western blotting substrate or West Pico PLUS chemiluminescent substrate following manufacturer's protocols. The signal from the blots was detected using the ChemiDoc Imaging System (Bio-Rad, USA) and densitometric analysis was quantified by ImageJ software.

HPLC analysis

Tumor samples collected in the drug biodistribution study were weighed and homogenized on ice. Plasma and tumor homogenates were extracted in methanol, using 1:4 and 1: 3 v/v dilutions, respectively. After vortexing 20 s and centrifugation at 13,000 rpm for 10 min, the Nintedanib-containing supernatants were filtered through 0.22 μm filters for HPLC analysis. The HPLC system was operated by a Knauer Smartline Pneumatic Pump, C18 column, K-2600 spectrophotometer, and Gina data acquisition software. Two mobile phases, mobile phase A (0.01% trifluoroacetic acid in water) and mobile phase B (0.01% trifluoroacetic acid in acetonitrile), where used as a 30/70% combination (v/v). 4 μL of the sample was injected to measure the Nintedanib absorption at 390 nm. The Nintedanib standard curve was generated up to a maximal concentration of 200 μg/mL.

Assessment of Nintedanib pharmacokinetics and biodistribution

A DiR-labeled Silicasome-Nintedanib was prepared for *in vivo* and *ex vivo* imaging, following IV administration. Nintedanib esylate was dissolved in a vehicle (20% HP-β-CD in saline) before oral administration. All animal experimental protocols were approved by the UCLA Animal Research Committee. An orthotopic KPC-luc tumor model was established in immunocompetent B6129SF1/J mice, as previously described by us [11]. Briefly, 40 μL DMEM/Matrigel (1:1 v/v), containing 8×10^5 KPC-luc cells, was injected into the pancreas tail of 9-week old female B6129SF1/J mice, using a small surgical procedure under anesthesia. 15 days after the orthotopic tumor implantation, tumor-bearing mice were randomly assigned into different groups, which received one IV injection of saline or Silicasome-Nintedanib-DiR, as well as one oral administration of free Nintedanib, respectively. The dose equivalent of Nintedanib was 50 mg/kg. Blood samples, primary tumors or major organs were collected after the specific time points.

For the performance of Nintedanib PK study, blood samples (n = 3) were collected at 10 min, 30 min, 1 h, 3 h, 9 h, and 24 h post-injection, and the plasma was obtained by centrifuging at 3500 rpm for 20 min. Free Nintedanib was extracted by methanol and measured by HPLC analysis.

For the assessment of nanocarrier biodistribution, the *in vivo* fluorescence intensity of Silicasome-Nintedanib-DiR group (n = 3) was assessed in a Xenogen IVIS imaging system, 24, 48 and 72 h after IV injection. Following animal sacrifice, tumors and major organs were harvested for *ex vivo* IVIS imaging and quantitative analysis.

For the assessment of drug biodistribution, tumors (n = 3) were collected at 24, 48 and 72 h post-injection from saline, free Nintedanib and Silicasome-Nintedanib-DiR groups. HPLC analysis was used to determine the Nintedanib content of tumors.

Assessment of the therapeutic efficacy in the orthotopic KPC-luc tumor model

A 40 μL suspension of DMEM/Matrigel (1:1 v/v), containing 8×10^5 KPC-luc cells, was injected into the pancreas tail of 9-week old female B6129SF1/J mice as described above. After 6 days, IVIS imaging was used to confirm the establishment of bioluminescent tumors. Animals were randomly assigned into 3 groups (n = 6), which received IV injection of

saline, oral administration of free Nintedanib, and IV injection of Silicasome-Nintedanib, respectively, twice a week for 2 weeks. The dose equivalent of Nintedanib was 50 mg/kg per dose. Nintedanib esylate was dissolved in a vehicle (20% HP-β-CD in saline) before oral administration. Animal weight was monitored every 2 days.

Bioluminescence imaging of the luciferase-expressing tumors was performed on day 5, 12, and 16 by intraperitoneal injection with 50 mg/kg D-Luciferin. Tumors were collected from sacrificed animals on day 21. Photographs and weights of the harvested tumors were obtained before separation into 2 parts. One tumor piece was frozen at − 80 °C for Western blotting to determine p-ERK expression, as described above. The other tumor piece was fixed in 10% formalin for the performance of IHC staining by the UCLA Translational Pathology Core Laboratory. IHC analysis was performed to assess tumor staining intensity for CD31, CD8, FoxP3, PD-L1, and p-ERK. Image processing was performed using Aperio ImageScope software (Leica).

Assessment of the synergistic immunotherapy efficacy by combining Si-Ninte with αPD-1 in the orthotopic KPC-luc tumor model

A 40 μL suspension of DMEM/Matrigel (1:1 v/v), containing 8×10^5 KPC-luc cells, was injected into the pancreas tail of 9-week-old female B6129SF1/J mice, as described above. After 6 days, IVIS imaging was used to confirm the establishment of bioluminescent tumors. Animals were randomly assigned into 4 groups (n = 6) which received twice weekly IV injections of saline, IP injection of free αPD-1, IV injection of Silicasome-Nintedanib, or IV injection of Silicasome-Nintedanib plus IP injection of free αPD-1, respectively, for 2 weeks. αPD-1 was dissolved in a dilution buffer (pH 7) before the IP injection, according to manufacturer's instructions. The dose equivalent of Nintedanib was 50 mg/kg per animal. Animal weight was monitored every 2 days.

To perform the bioluminescence imaging, mice were injected intraperitoneal with 50 mg/kg D-Luciferin on day 6, 12, 16, and 19. Tumors were collected from sacrificed animals on day 19. Photographs and tumor weights were obtained, before fixing in 10% formalin. IHC analysis was performed to assess tumor staining intensity for CD31, CD8, FoxP3, and PD-L1.

Statistical analysis

Differences among groups were estimated by one-way ANOVA analysis. Data were expressed as mean ± standard deviation (SD), representing at least three independent experiments. A statistically significant difference was considered at *$p < 0.05$; **$p < 0.01$; #$p < 0.05$ and ##$p < 0.01$, as indicated in the figure legends.

Results

Development of the silicasome platform for delivery of the tyrosine protein kinase inhibitor, Nintedanib

Nintedanib is an effective TPK inhibitor of the VEGF, PDGF, and FGF receptors that are expressed at the PDAC site. Not only does this allow the possibility to intervene in the

tumor dysplasia but can also be used to improve vascular delivery and the tumor immune landscape, which are negatively impacted by the stroma. To achieve this objective, it was necessary to consider the stroma hindrance of the delivery of a relatively hydrophobic drug that makes it past the rigorous stroma-vascular barrier in PDAC. We have previously demonstrated the effective utilization of mesoporous silica nanoparticles (MSNPs), coated with a lipid bilayer, to overcome this challenge by transcytosis uptake at the PDAC site [11]. Upon considering silicasome use for Nintedanib delivery the medicinal chemistry characteristics of the drug was investigated, showing a low water solubility index of 0.03 mg/ml and weak basic properties (pKa = 7.23; LogP = 2.79). The latter characteristic was exploited for testing drug loading after encapsulation a proton-generating trapping agent in the silicasome pores (Fig. 1). To test whether proton release from $(NH_4)_2SO_4$ can accomplish this objective, a liposomal lipid bilayer was used, to test the feasibility of drug import (Fig. S1a and b). Liposomes were constructed by a microfluidics approach, requiring the mixing and blending an organic phase, containing ethanol-dissolved lipids (DSPC/Chol/DSPE-PEG2000) in a molar ratio of 60:40:3, with an aqueous phase containing the trapping agent, ammonium sulfate (Fig. S1a and b). This yielded 74.2 ± 0.9 nm vesicles for incubation in a HEPES buffer (5 mM HEPES, 5% dextrose, pH 6), in which Nintedanib esylate was dissolved. This accomplished an effective drug loading capacity of 22.6% in what we designated a Liposome-Nintedanib carrier. Cryo-electron microscopy (CryoEM) was used to confirm the construction of liposomes, containing an internal drug precipitate (Fig. S1c).

Successful completion of liposome construction was followed by the synthesis of a silicasome carrier (Fig. 1a). Spherical MSNPs were synthesized and used for soaking in the trapping agent, triethylammonium sucrose octasulfate (TEA_8SOS) [11], [12]. The lipid bilayer was applied by sonicating the MSNPs in a lipid solution of similar composition as the liposomes, including the presence of 2000 kDa polyethylene glycol (PEG_{2000}) (Fig. 1a). Following removal of the unencapsulated trapping agent, Nintedanib, remote loading was achieved with the drug dissolved in a HEPES buffer, yielding a loading capacity of 32.8% (Fig. 1b). The Silicasome-Nintedanib carrier, also designated Si-Ninte, was purified by washing in a HEPES-buffered NaCl solution. CyroEM confirmed the encapsulation and integrity of the particles with a coated and supported lipid bilayer (Fig. 2c). Hydrodynamic size measurement showed a carrier with a diameter of 125.9 ± 2.0 nm, a pore size of ~3.76 nm and a zeta potential of − 8.0 ± 2.8 mV (Fig. 1c). Although we have not performed drug release profiling for Nintedanib from the silicasome, we have previously demonstrated 20-24% of both irinotecan and AZD1080 are released from this carrier over 4 h in an acidic environment, while amounting to ~5% drug release at a pH of 7.4 [13], [24]

Si-Ninte pharmacokinetics (PK) and drug delivery at an orthotopic PDAC tumor site

PK analysis and carrier biodistribution was carried out by a nanocarrier incorporating an infrared fluorescent cyanine dye, DiR, into the lipid bilayer. The physicochemical characteristics of this carrier, designated Si-Ninte-DiR, are shown in Fig. 2c. To establish a robust tumor model with a dysplastic stroma and growth characteristics resembling human PDAC, we used luciferase-expressing Kras pancreatic cancer (KPC) cells, previously established from a tumor harvested from a transgenic Pdx1-cre/LSL-Kras G12D/p53R172H

animal. The cells were injected into the pancreatic tail of immunocompetent B6129SF1/J mice to establish an orthotopic KPC-luc tumor model for assessment of PK and drug biodistribution (Fig. 2a). Fifteen days after KPC implantation, the tumor bearing mice were divided into three groups. The first group received a single intravenous (IV) injection of saline, the second group received a single oral dose of free Nintedanib (50 mg/kg), and the third group received a single IV injection of Si-Ninte-DiR (Ninte, 50 mg/kg). This was followed by collecting plasma samples at 6 intervals over a 24-hour period, followed by animal sacrifice and harvesting of tumors and major organs for further analysis. The plasma samples (n = 3) were used to assess the circulatory Nintedanib concentrations, using HPLC (Fig. 2d). This analysis demonstrated a noticeable contrast in the clearance of free Ninte, administered orally, compared to the encapsulated drug concentration in the blood. Thus, while free Ninte was rapidly cleared, the encapsulated drug was retained at high blood levels for at least 24 hours, indicating a significant improvement in PK (Fig. 2d).

In vivo IVIS imaging of the DiR-labeled Si-Ninte carrier (n = 3), obtained after 24, 48, and 72 h, revealed effective biodistribution to the abdominal region (Fig. 2e). Following animal sacrifice and performing *ex vivo* explantation of tumor tissues and the major organs, carrier biodistribution could be observed at the primary tumor site as well as the heart, lung, liver, stomach, spleen, intestines, and kidney. DiR fluorescence intensity was used for quantifying the biodistribution to these delivery sites, as depicted in Fig. 2e (right-side panel) and Fig. S2. The data in Fig. 2f demonstrates that tumor site distribution after 24, 48, and 72 h accounted for 25.5%, 25.1%, and 17.1% of the injected carrier amount, respectively. There was also prominent biodistribution to the liver, amounting to 40.1%, 40.4%, and 47.1% of the injected dose, respectively. These results are indicative of the liver's significant contribution to particle sequestration by phagocytic uptake (slowed down by surface PEGylation). Additionally, some fluorescence intensity was observed in the vicinity of the intestines and spleen, which reflect sites of metastatic spread and possible participation in the immune response (e.g., the spleen).

The tumor samples (n = 3) collected after 24, 48 and 72 were used to assess Nintedanib content by HPLC analysis. This demonstrated that the Nintedanib tissue dose in the Si-Ninte-DiR treated group was 20.82, 6.50 and 3.24 μg/g, respectively, in comparison to 0.33, 0.43 and 0.03 μg/g in the orally administered Ninte group (Fig. 2g). This indicates that encapsulated delivery improves the drug levels 63-fold (20.82/0.33), 15-fold (6.50/0.43) and 108-fold (3.24/0.03), respectively, after 24, 48 and 72 h (Fig. 2g). These results agree with improvement in the PK profile (Fig. 2d).

Impact of encapsulated drug delivery on the vasculature and immune landscape at the PDAC site

Nintedanib, a triple PTK inhibitor, is primarily used for the treatment of pulmonary fibrosis, targeting growth factor receptors in the lung. However, the drug also interferes with signaling pathways related to angiogenesis, with the potential to impact growth of cancer cells and TME, where the stroma and ECM deposition impact blood vessel permeation and the immune landscape. The interference in VEGFR, PDGFR and FGFR signaling pathways by Nintedanib has been well established, providing the benefit of blocking overexpression

of these receptors in the PDAC TME [18], [25]. Considering the dramatic improvement of encapsulated Nintedanib delivery at the PDAC site, we focused the vasculature, and immune landscape. A further orthotopic experiment was performed (Fig. 3a) to follow orthotopic KPC tumor growth (Fig. 3b). These animals (n = 6 mice per group) received either an IV injection of saline, oral administration of free Nintedanib (50 mg/kg), or an IV injection of Si-Ninte (10 mg/kg), twice a week for 2 weeks (Fig. 3a). *In vivo* IVIS imaging was performed on days 6, 12, and 16 to quantify tumor bioluminescence intensity on days 12 and 16 (Fig. 3b). This demonstrated a significant decrease in the luminescence intensity in the Si-Ninte treated group, which was significantly lower ($p < 0.05$) than for the saline and free Nintedanib groups (Fig. 3c). Moreover, tumor harvesting from sacrificed animals on day 21 showed that both the tumor weights (Fig. 3d) and observable tumor sizes (Fig. 3e) were significantly reduced in the Si-Ninte group compared to the other treatments.

The harvested primary tumors were subjected to IHC analysis to study some of the TME characteristics. The assessment of CD31 staining intensity demonstrated a significant reduction in vascular density following Si-Ninte administration, compared to saline or free drug treatment (Fig. 4a). In addition, Trichome staining to assess collagen density demonstrated a 1.4-fold and 4.8-fold decrease in the deposition of this extracellular matrix component, following treatment with Free Ninte and Si-Ninte, compared to saline (Fig. 4b). This stromal impact, accompanied by improved drug delivery to the TME (Fig. 2g), suggests that the actual reduction in vascular density may be accompanied by increased vascular permeability. The possible explanation for this finding is that Nintedanib improves the structural abnormality that underpins blood vessel permeation at the PDAC site and other cancer sites [22]. This is also referred to as vascular normalization, a potentially valuable therapeutic response to improve tumor perfusion, reduction of hypoxia and enhancing drug delivery [26].

Several preclinical studies have highlighted the potential of Nintedanib having a beneficial effect on immune recruitment to the TME, and the possibility of impacting anti-tumor immunity. For instance, Kato *et al.* demonstrated that Nintedanib interferes with the proliferation and immune suppressive activity of cancer-associated fibroblasts (CAFs) in a murine melanoma model, where the response was accompanied by increased recruitment of activated $CD8^+$ T cells [27]. To evaluate whether Nintedanib influences the orthotopic PDAC TME, IHC analysis was performed to assess $CD8^+$ CTL recruitment to both the tumor margins and core, as depicted in Fig 4c. Remarkably, the results demonstrated that both free Ninte and Si-Ninte significantly enhanced $CD8^+$ T-cell recruitment to the tumor margins and cores, compared to saline treatment. Notably, Si-Ninte exhibited the most robust effect. We also performed IHC analysis to discern the presence of regulatory T-cells (Tregs), which play a crucial role in the immune suppressive PDAC landscape, by assessing $FoxP3^+$ expression. This analysis showed a significant reduction in Treg cell infiltration following Si-Ninte treatment compared to other treatments (Fig. 4d and Fig. S4). Additionally, expression of the number of $CD8^+$ to $FoxP3^+$ T-cells revealed the largest ratio increases for Si-Ninte compared to the other treatment groups (Fig. 4f).

Nintedanib impacts the PD-L1 expression in vitro and in vivo

There is growing evidence in preclinical melanoma, colon, lung, and triple negative breast cancer models in animals that, in addition to improved $CD8^+$ CTL recruitment, anti-angiogenic drugs also impact the CTL activation status by changing checkpoint receptor expression, with the possibility to boost the immune response by checkpoint blocking antibodies [22], [27]. To investigate whether encapsulated Nintedanib exert an effect on PD-L1 expression, IHC analysis was performed on tumors from the orthotopic KPC model (Fig. 3a). The revealed that both free and encapsulated Nintedanib could increase PD-L1 expression (Fig. 5a), with Si-Ninte exhibiting a more robust effect ($p = 0.04$). To understand the mechanism leading to increased PD-L1 expression, *in vitro* analysis was carried out in KPC cells, which were treated with 0.5 or 1 μM free Ninte or Si-Ninte for 24 hours before assessing surface PD-L1 expression by flow cytometry (Fig. 5b, left-panel). Both free and encapsulated drug versions increased PD-L1 expression, congruent with the *in vivo* data. From this perspective, it is known that biological stimuli leading to PD-L1 expression engage signaling pathways that are responsible for transcriptional activation of the gene promoter in the TME (Fig. 5c). These stimuli include cytokines (e.g., IFN-γ), toll-like receptor ligands (e.g., nucleic acids acting as danger signals), oncogenic signaling pathways (e.g., RAS) and hypoxia, acting on signaling pathways that impact the IFN-γ-activated sequence (GAS) element, nuclear factor-kappa B (NF-κB), activator protein 1 (AP1) and hypoxia-inducible factor 1 (HIF-1) binding sites in the PD-L1 promotor [28], [29], [30]. We chose recombinant IFN-γ to assess the impact on PD-L1 expression in KPC cells during flow cytometry analysis (Fig. 5b, right side panel). Noteworthy, this response was significantly boosted by the addition of 0.5-1 μM free or encapsulated Nintedanib, suggesting that the drug augments the impact of the cytokine-induced STAT activation pathway.

To elucidate a possible signaling pathway engaged by Nintedanib in PDAC tumors, it is known the impacted growth factor receptors in the TME converge on the mitogen activated protein kinase (MAPK), Janus kinase/signal transducers and activators of transcription (JAK/STAT), and phosphatidylinositol 3-kinase (PI3K) signaling pathways (Fig. 5c) [31]. Not only is there intensive crosstalk between these pathways at multiple levels, but also involve compensatory feedback mechanisms that determine net response outcome [31]. As an example, it has been reported that Nintedanib differentially impact extracellular receptor kinase (ERK) signaling in different PDAC cell lines [32]. Accordingly, we focused on the phosphorylation of ERK1 and ERK2, which controls the activation of this kinase. This was accomplished by determining phospho-ERK status in KPC cells and orthotopic KPC tumors. The phosphorylation of STAT3 (pSTAT3) was used for comparing cytokine signaling. To assess the phosphorylation status of ERK1/ ERK2 and STAT3 by Nintedanib, the first experiment was undertaken in KPC cells, treated with free Ninte or Si-Ninte. Cellular extracts were obtained for anti-phosphopeptide immunoblotting. This was accomplished by electrophoretic separation of proteins, which were transferred onto nitrocellulose membranes. The membranes were overlaid by antibodies that recognize total ERK1/2 (tERK), phospho-ERK1/2 (pERK), total STAT3 (tSTAT3) and phospho-STAT3 (pSTAT3) (Fig. 5d and Fig. S5). Vinculin served as a stable-expressed household protein for comparative analysis. Visual inspection as well as protein scanning density analysis

demonstrated a significant increase in the phosphorylation of ERK in relation to the total ERK or vinculin protein levels in response to both free and encapsulated drug treatment (Fig. 5d). However, there was no increase in the level of STAT3 phosphorylation by either treatment (Fig. S5).

To validate whether the *in vitro* findings align with the *in vivo* outcome, we also conducted IHC and phosphopeptide immunoblotting analyses on tumor slices and protein extracts obtained from the orthotopic tumors in Fig. 4. The IHC analysis revealed statistically significant increases in pERK staining intensity during treatment with both free and encapsulated Nintedanib (Fig. 5e). While there was no significant change in the overall pERK staining intensity for free versus the encapsulated drug, we did observe increased nuclear localization of pERK in in response to treatment with the encapsulated drug. Nuclear localization is important for activation of c-Jun and c-Fos and the subsequent interaction with the AP1 binding site in the promoter. These results were further supported by a significant increase in the phosphorylation of ERK in the protein extracts obtained free and encapsulated Nintedanib (Fig. 5f). In summary, the combined *in vitro* and *in vivo* analyses provide valuable insight on ERK activation and PD-L1 expression by Nintedanib. This prompted a question as to whether checkpoint blocking antibodies can be used to further enhance the immune effect.

Combination therapy with Si-Ninte plus anti-PD-1 (αPD-1) enhances anti-PDAC immunity

Based on the observed increase in PD-L1 expression in response to Si-Ninte treatment, we hypothesized that the combination of anti-PD1 (αPD-1) immunotherapy and Si-Ninte could be used to boost the immune response in the orthotopic KPC model. To test this hypothesis, we established orthotopic growing tumors in the animals (n = 6 per group) and administered different treatments for a span of two weeks. These included twice-weekly IV injection of saline, IP injection of αPD-1 (10 mg/kg), IV injection of Si-Ninte (10 mg/kg), or IV injection of the same dose of the carrier along with IP αPD-1 (10 mg/kg) (Fig. 6a). Throughout the treatment period, we monitored tumor growth by IVIS imaging on days 6, 12, 16, and 19 (Fig. 6b). Quantitative analysis of tumor bioluminescence intensity on days 12, 16, and 19 demonstrated a significant luminescence reduction in mice treated with Si-Ninte (with or without αPD-1), compared to saline or free αPD-1 (Fig. 6c). Moreover, the combination therapy showed a statistically significant effect compared to monotherapy, indicating synergistic benefit from combining anti-angiogenesis therapy and immune checkpoint therapy. These findings were further confirmed by tumor weight assessment and photographic images of the tumors (Fig. 6d).

Following animal sacrifice on day 19, primary tumors were harvested for IHC analysis of the immune landscape. The assessment of PD-L1 expression revealed increased staining intensity in response to Si-Ninte treatment, with or without αPD-1, compared to the saline control or αPD-1 alone (Fig. 6e and Fig. S7a). We also analyzed CD8 and FoxP3 expression (Fig. 6e, Fig. S7b and Fig. S7c), which demonstrated that combination therapy resulted in the highest density of $CD8^+$ T-cell recruitment along with the most significant decline in Treg cell numbers at the tumor site. These results correlated with a statistically significant

increase in the ratio of $CD8^+$ to $FoxP3^+$ cells after combination therapy, compared to the monotherapies (Fig. 6e and Fig. S7d).

In conclusion, the combination of Si-Ninte with αPD-1 showed promising results in enhancing the antitumor response in the orthotopic KPC model, supported by changes in PD-L1 expression and the immune landscape of the tumors. These findings suggest the potential of synergistic effects when combining anti-angiogenesis therapy and immune checkpoint therapy in the treatment of pancreatic cancer.

Discussion

In this study, we introduce a novel approach to enhance the effectiveness of Nintedanib, a triple PTK inhibitor targeting VEGFR, PDGFR, and FGFR. Our method involves remote loading Nintedanib into the pores of a lipid-bilayer coated mesoporous silica nanocarrier, known as silicasome. Through this approach, we demonstrate improved pharmacokinetics and efficient drug delivery to a dysplastic, orthotopic PDAC tumor model in which PTK receptors are overexpressed. The incorporation of Nintedanib into the nanocarrier had significant effects on vascular pruning and normalization, allowing significant impact on the dysplastic stroma. This is evident from the reduction in CD31 and collagen staining intensities, suggesting a more responsive TME. The response was accompanied by a robust antitumor immune response, as reflected by tumor shrinkage, increased infiltration of $CD8^+$ T-cells in tumor margins and cores, as well as reduced Treg infiltration. Further *in vitro* and *in vivo* experiments unveiled Nintedanib's ability to upregulate PD-L1expression, with assistance of the ERK pathway. This allowed additional boosting of the immune response when the dual delivery carrier was combined with anti-PD1 treatment. In summary, our findings underscore the positive effects of improved drug delivery to the PDAC stroma by the silicasome carrier, in addition to an impact on antitumor immunity by the PTK inhibitor. Accordingly, the encapsulated delivery of Nintedanib holds significant promise for advancing the impact of immunotherapy approaches for pancreatic cancer.

The major finding of our research contribution is the use of a nanocarrier to improve the delivery of a PTK inhibitor, which impacts PDAC stromal composition, vasculature, and the anti-tumor immunity. This is important from the perspective of how the abundant dysplastic stroma impacts drug delivery and contributing to an immunosuppressive environment. From a disease context, this also provides a major reason why Nintedanib, commonly used as an oral agent, was encapsulated in a nanocarrier to overcome the stromal-vascular barrier that hinders drug delivery at the PDAC site, as confirmed by our PK and biodistribution study comparing encapsulated with oral administered free Nintedanib (Fig. 2g). Use of the silicasome led to a dramatic improvement in circulatory half-life as well as drug content at the orthotopic tumor site. This is the first demonstration, to our knowledge, have nanocarrier use to improve Nintedanib delivery to a disease site *in vivo*. Our finding also corroborates the use of nanocarriers for other poorly soluble PTK inhibitors to improve PK and drug delivery, including for polymer nanoparticles and liposomes delivering apatinib or nanocarrier for delivering of sorafenib [33], [34], [35].

While several approaches have been implemented to decrease the impact of the dysplastic stroma on drug delivery and anti-PDAC immune defense, the use of PTK inhibitors is a recent introduction to PDAC stromal therapeutics, which also include pegylated hyaluronidase (PEGPH20) to deplete hyaluronic acid, collagenase for collagen depletion, or inhibitors for TGF-β inhibitors or the angiotensin system [36], [37], [38], [39]. An example of a small molecule PTK inhibitor is 7rh, which interferes with discoidin domain receptor 1 (DDR1) signaling in response to collagen binding, allowing for a therapeutic impact on stromal desmoplasia, tumor cell invasion and metastasis in PDAC [40]. Another example is ibrutinib, a Bruton's to PK inhibitor, which decreased collagen deposition and desmoplasia in animal PDAC tumor models [41]. We extend these findings with the use of a triple-PTK inhibitor showing several impacts on the orthotopic PDAC stroma, benefiting drug delivery and immune defense (Fig. 4b).

One major benefit in our study was the reduction of vascular (CD31) density, which was accompanied by improved drug delivery. This combination suggests actual structural change in the tumor vasculature to allow for increased permeability of the Nintedanib carrier. This concept is also known as vascular normalization, which refers to a therapeutic strategy aimed at improving the abnormal and chaotic blood vessel structure within the TME [42]. In many solid tumors, including pancreatic cancer, the blood vessels supplying nutrients and oxygen are often disorganized, leaky, and inefficient, contributing to therapeutic resistance, aggressive growth, and metastasis [43], [44]. Several strategies have been developed for vascular normalization by targeting PTK receptors, including monoclonal antibodies and small molecule PTK inhibitors [45], [46], [47]. Notably, PTK inhibitors show competition with the ATP binding site of the kinase catalytic domain, with some of the agents capable of binding to multi-kinase receptors with broad spectra of activity. Sunitinib, a PTK inhibitor targeting VEGFR and PDGFR, was confirmed to loosen the pericyte attachment to endothelial cells, altering the tortuous vascular structure [48]. Similarly, Nintedanib have been reported to reduce the average vessel density, with an increase of the α-SMA$^+$/CD31$^+$ ratio in colon tumors, demonstrating the capacity towards tumor vascular normalization [22]. All considered, PTK inhibitors are poised to expand the therapeutic use effects of steroids to achieve tumor vascular normalization.

Finally, a major benefit of using the silicasome for Nintedanib delivery was to improve anti-PDAC immunity in a rigorous orthotopic tumor model. One possible contribution by the PTK inhibitor is to reduce the physical barrier to T-cell recruitment to the desmoplastic stroma, leading to a significant increase in CD8$^+$ T-cell infiltration in the tumor margin as well as the tumor core (Fig. 4c). Another possible contribution is impacting the biological effects of the PDAC stroma on the recruitment immunosuppressive cells, such as Tregs. Noteworthy Nintedanib delivery had a significant effect on reducing Tregs and increasing the CD8$^+$/Treg ratio at the tumor site (Fig. 4d). Accordingly, we propose that this combination of increased tumor cell lysis and elimination of immune suppressive effects contributed to shrinking of primary tumors and metastasis reduction in our orthotopic PDAC model.

An interesting feature of the altered immune landscape was the increase in PD-L1 expression by Nintedanib through an impact on the ERK pathway (Fig. 5d-f). This allowed

boosting of the drug effect on immunotherapy by the addition of an anti-PD-1 monoclonal antibody (Fig. 6e). These findings agree with the demonstration that Nintedanib treatment could also boost anti-PD-L1 immunotherapy in preclinical melanoma, colon, lung cancer and triple negative breast cancer tumor models [22], [27]. The impact on the ERK pathway is interesting from the perspective that this pathway is differentially affected by PTK inhibitors in a variety of pancreatic cancer cell types [30]. This contrasts with the Nintedanib impact on the STAT3 pathway in other cancer types as reported by Tu *et al.* [22].

In conclusion, our studies indicate that encapsulated delivery of Nintedanib, hold several advantages for interfering in the dysplastic stroma of PDAC, both from the perspective of carrier efficacy for improving drug delivery at the difficult to reach tumor site, as well as the specific pharmacological properties of the PTK inhibitor. Thus, it is possible to envisage combining Nintedanib with additional immune modulators in the silicasome carrier, including drugs that can be incorporated into the lipid bilayer, e.g., paclitaxel, a TLR7 agonist, an IDO-1 prodrug inhibitor, or a PD-1 prodrug inhibitor. Moreover, immune modulatory therapy by the silicasome can also be combined with chemotherapeutic agents that exhibit immunogenic properties, such as irinotecan, oxaliplatin, DCH-Pt, doxorubicin and mitoxantrone [7].

Supplementary Material

Refer to Web version on PubMed Central for supplementary material.

Acknowledgment

This study was supported by the U.S. Public Health Service Grant, R01CA247666-03. The authors thank the Preclinical Imaging Technology Center, the Electron Imaging Center for Nanomachines (EICN), the Translational Pathology Core Laboratory (TPCL), the Molecular Instrumentation Center, and the CNSI Advanced Light Microscopy/Spectroscopy (ALMS) Shared Facility at UCLA.

Abbreviations

PDAC	Pancreatic ductal adenocarcinoma
PTK	Protein tyrosine kinase
PK	Pharmacokinetics
KPC	KRAS-mediated pancreatic carcinoma
ERK	Extracellular signal-regulated kinase
ECM	Extracellular matrix
CAFs	Cancer-associated fibroblasts
TME	Tumor microenvironment
MSNPs	Mesoporous silica nanoparticles
VEGF	Vascular endothelial growth factor

PDGF	Platelet-derived growth factor
FGF	Fibroblast growth factor
Tregs	Regulatory T-cells
STAT	Signal transducers and activators of transcription

References

[1]. Siegel RL, Miller KD, Wagle NS, Jemal A, Cancer statistics, 2023, CA Cancer J. Clin 73 (2023) 17–48. 10.3322/caac.21763. [PubMed: 36633525]

[2]. Erkan M, Hausmann S, Michalski CW, Fingerle AA, Dobritz M, Kleeff J, Friess H, The role of stroma in pancreatic cancer: diagnostic and therapeutic implications, Nat. Rev. Gastroenterol. Hepatol 9 (2012) 454–467. 10.1038/nrgastro.2012.115. [PubMed: 22710569]

[3]. Hosein AN, Brekken RA, Maitra A, Pancreatic cancer stroma: an update on therapeutic targeting strategies, Nat. Rev. Gastroenterol. Hepatol 17 (2020) 487–505. 10.1038/s41575-020-0300-1. [PubMed: 32393771]

[4]. Meng H, Nel AE, Use of nano engineered approaches to overcome the stromal barrier in pancreatic cancer, Adv. Drug Deliv. Rev 130 (2018) 50–57. 10.1016/j.addr.2018.06.014. [PubMed: 29958925]

[5]. Liu L, Kshirsagar PG, Gautam SK, Gulati M, Wafa EI, Christiansen JC, White BM, Mallapragada SK, Wannemuehler MJ, Kumar S, Solheim JC, Batra SK, Salem AK, Narasimhan B, Jain M, Nanocarriers for pancreatic cancer imaging, treatments, and immunotherapies, Theranostics. 12 (2022) 1030–1060. 10.7150/thno.64805. [PubMed: 35154473]

[6]. Ortíz R, Quiñonero F, García-Pinel B, Fuel M, Mesas C, Cabeza L, Melguizo C, Prados J, Nanomedicine to Overcome Multidrug Resistance Mechanisms in Colon and Pancreatic Cancer: Recent Progress, Cancers. 13 (2021) 2058. 10.3390/cancers13092058. [PubMed: 33923200]

[7]. Nel AE, Mei K-C, Liao Y-P, Liu X, Multifunctional Lipid Bilayer Nanocarriers for Cancer Immunotherapy in Heterogeneous Tumor Microenvironments, Combining Immunogenic Cell Death Stimuli with Immune Modulatory Drugs, ACS Nano. 16 (2022) 5184–5232. 10.1021/acsnano.2c01252. [PubMed: 35348320]

[8]. Frampton JE, Liposomal Irinotecan: A Review in Metastatic Pancreatic Adenocarcinoma, Drugs. 80 (2020) 1007–1018. 10.1007/s40265-020-01336-6. [PubMed: 32557396]

[9]. Von Hoff DD, Ervin T, Arena FP, Chiorean EG, Infante J, Moore M, Seay T, Tjulandin SA, Ma WW, Saleh MN, Harris M, Reni M, Dowden S, Laheru D, Bahary N, Ramanathan RK, Tabernero J, Hidalgo M, Goldstein D, Van Cutsem E, Wei X, Iglesias J, Renschler MF, Increased Survival in Pancreatic Cancer with nab-Paclitaxel plus Gemcitabine, N. Engl. J. Med 369 (2013) 1691–1703. 10.1056/NEJMoa1304369. [PubMed: 24131140]

[10]. Liu X, Lin P, Perrett I, Lin J, Liao Y-P, Chang CH, Jiang J, Wu N, Donahue T, Wainberg Z, Nel AE, Meng H, Tumor-penetrating peptide enhances transcytosis of silicasome-based chemotherapy for pancreatic cancer, J. Clin. Invest 127 (2017) 2007–2018. 10.1172/JCI92284. [PubMed: 28414297]

[11]. Liu X, Situ A, Kang Y, Villabroza KR, Liao Y, Chang CH, Donahue T, Nel AE, Meng H, Irinotecan Delivery by Lipid-Coated Mesoporous Silica Nanoparticles Shows Improved Efficacy and Safety over Liposomes for Pancreatic Cancer, ACS Nano. 10 (2016) 2702–2715. 10.1021/acsnano.5b07781. [PubMed: 26835979]

[12]. Liu X, Jiang J, Chan R, Ji Y, Lu J, Liao Y-P, Okene M, Lin J, Lin P, Chang CH, Wang X, Tang I, Zheng E, Qiu W, Wainberg ZA, Nel AE, Meng H, Improved Efficacy and Reduced Toxicity Using a Custom-Designed Irinotecan-Delivering Silicasome for Orthotopic Colon Cancer, ACS Nano. 13 (2019) 38–53. 10.1021/acsnano.8b06164. [PubMed: 30525443]

[13]. Liu X, Jiang J, Liao Y-P, Tang I, Zheng E, Qiu W, Lin M, Wang X, Ji Y, Mei K-C, Liu Q, Chang CH, Wainberg ZA, Nel AE, Meng H, Combination Chemo-Immunotherapy for Pancreatic Cancer Using the Immunogenic Effects of an Irinotecan Silicasome Nanocarrier Plus Anti-PD-1, Adv. Sci 8 (2021) 2002147. 10.1002/advs.202002147.

[14]. Luo L, Wang X, Liao Y-P, Chang CH, Nel AE, Nanocarrier Co-formulation for Delivery of a TLR7 Agonist plus an Immunogenic Cell Death Stimulus Triggers Effective Pancreatic Cancer Chemo-immunotherapy, ACS Nano. (2022). 10.1021/acsnano.2c06300.

[15]. Lakkakula BVKS, Farran B, Lakkakula S, Peela S, Yarla NS, Bramhachari PV, Kamal MA, Saddala MS, Nagaraju GP, Small molecule tyrosine kinase inhibitors and pancreatic cancer—Trials and troubles, Semi. Cancer Bio 56 (2019) 149–167. 10.1016/j.semcancer.2018.09.011.

[16]. Fujimoto K, Hosotani R, Wada M, Lee J-U, Koshiba T, Miyamoto Y, Tsuji S, Nakajima S, Doi R, Imamura M, Expression of two angiogenic factors, vascular endothelial growth factor and platelet-derived endothelial cell growth factor in human pancreatic cancer, and its relationship to angiogenesis, Eur. J. Cancer 34 (1998) 1439–1447. 10.1016/S0959-8049(98)00069-0. [PubMed: 9849429]

[17]. Ohta T, Yamamoto M, Numata M, Iseki S, Tsukioka Y, Miyashita T, Kayahara M, Nagakawa T, Miyazaki I, Nishikawa K, Yoshitake Y, Expression of basic fibroblast growth factor and its receptor in human pancreatic carcinomas, Br. J. Cancer 72 (1995) 824–831. 10.1038/bjc.1995.420. [PubMed: 7547227]

[18]. Hilberg F, Roth GJ, Krssak M, Kautschitsch S, Sommergruber W, Tontsch-Grunt U, Garin-Chesa P, Bader G, Zoephel A, Quant J, Heckel A, Rettig WJ, BIBF 1120: Triple Angiokinase Inhibitor with Sustained Receptor Blockade and Good Antitumor Efficacy, Cancer Res. 68 (2008) 4774–4782. 10.1158/0008-5472.CAN-07-6307. [PubMed: 18559524]

[19]. Fala L, Ofev (Nintedanib): First Tyrosine Kinase Inhibitor Approved for the Treatment of Patients with Idiopathic Pulmonary Fibrosis, Am. Health Drug Benefits. 8 (2015) 101–104. [PubMed: 26629273]

[20]. Raghu G, Rochwerg B, Zhang Y, Garcia CAC, Azuma A, Behr J, Brozek JL, Collard HR, Cunningham W, Homma S, Johkoh T, Martinez FJ, Myers J, Protzko SL, Richeldi L, Rind D, Selman M, Theodore A, Wells AU, Hoogsteden H, Schünemann HJ, An Official ATS/ERS/JRS/ALAT Clinical Practice Guideline: Treatment of Idiopathic Pulmonary Fibrosis. An Update of the 2011 Clinical Practice Guideline, Am. J. Respir. Crit. Care Med 192 (2015) e3–e19. 10.1164/rccm.201506-1063ST. [PubMed: 26177183]

[21]. Flaherty KR, Wells AU, Cottin V, Devaraj A, Walsh SLF, Inoue Y, Richeldi L, Kolb M, Tetzlaff K, Stowasser S, Coeck C, Clerisme-Beaty E, Rosenstock B, Quaresma M, Haeufel T, Goeldner R-G, Schlenker-Herceg R, Brown KK, Nintedanib in Progressive Fibrosing Interstitial Lung Diseases, N. Engl. J. Med 381 (2019) 1718–1727. 10.1056/NEJMoa1908681. [PubMed: 31566307]

[22]. Tu J, Xu H, Ma L, Li C, Qin W, Chen X, Yi M, Sun L, Liu B, Yuan X, Nintedanib enhances the efficacy of PD-L1 blockade by upregulating MHC-I and PD-L1 expression in tumor cells, Theranostics. 12 (2022) 747–766. 10.7150/thno.65828. [PubMed: 34976211]

[23]. Wind S, Schmid U, Freiwald M, Marzin K, Lotz R, Ebner T, Stopfer P, Dallinger C, Clinical Pharmacokinetics and Pharmacodynamics of Nintedanib, Clin. Pharmacokinet. 58 (2019) 1131–1147. 10.1007/s40262-019-00766-0. [PubMed: 31016670]

[24]. Allen SD, Liu X, Jiang J, Liao Y-P, Chang CH, Nel AE, Meng H, Immune checkpoint inhibition in syngeneic mouse cancer models by a silicasome nanocarrier delivering a GSK3 inhibitor, Biomaterials. 269 (2021) 120635 10.1016/j.biomaterials.2020.120635 [PubMed: 33422940]

[25]. Hibi M, Kaneda H, Tanizaki J, Sakai K, Togashi Y, Terashima M, De Velasco MA, Fujita Y, Banno E, Nakamura Y, Takeda M, Ito A, Mitsudomi T, Nakagawa K, Okamoto I, Nishio K, FGFR gene alterations in lung squamous cell carcinoma are potential targets for the multikinase inhibitor nintedanib, Cancer Sci. 107 (2016) 1667–1676. 10.1111/cas.13071. [PubMed: 27581340]

[26]. Jain RK, Normalization of Tumor Vasculature: An Emerging Concept in Antiangiogenic Therapy, Science. 307 (2005) 58–62. 10.1126/science.1104819. [PubMed: 15637262]

[27]. Kato R, Haratani K, Hayashi H, Sakai K, Sakai H, Kawakami H, Tanaka K, Takeda M, Yonesaka K, Nishio K, Nakagawa K, Nintedanib promotes antitumour immunity and shows antitumour activity in combination with PD-1 blockade in mice: potential role of cancer-associated fibroblasts, Br. J. Cancer 124 (2021) 914–924. 10.1038/s41416-020-01201-z. [PubMed: 33299131]

[28]. Wang Y, Wang H, Yao H, Li C, Fang J-Y, Xu J, Regulation of PD-L1: Emerging Routes for Targeting Tumor Immune Evasion, Front. Pharmacol. 9 (2018). https://www.frontiersin.org/articles/10.3389/fphar.2018.00536.

[29]. Wu Y, Chen W, Xu ZP, Gu W, PD-L1 Distribution and Perspective for Cancer Immunotherapy —Blockade, Knockdown, or Inhibition, Front. Immunol 10 (2019). https://www.frontiersin.org/articles/10.3389/fimmu.2019.02022.

[30]. Yi M, Niu M, Xu L, Luo S, Wu K, Regulation of PD-L1 expression in the tumor microenvironment, J. Hematol. Oncol 14 (2021) 10. 10.1186/s13045-020-01027-5. [PubMed: 33413496]

[31]. Aksamitiene E, Kiyatkin A, Kholodenko BN, Cross-talk between mitogenic Ras/MAPK and survival PI3K/Akt pathways: a fine balance, Biochem. Soc. Trans 40 (2012) 139–146. 10.1042/BST20110609. [PubMed: 22260680]

[32]. Awasthi N, Hinz S, Brekken RA, Schwarz MA, Schwarz RE, Nintedanib, a triple angiokinase inhibitor, enhances cytotoxic therapy response in pancreatic cancer, Cancer Lett. 358 (2015) 59–66. 10.1016/j.canlet.2014.12.027. [PubMed: 25527450]

[33]. Li X, Wang L, Wang L, Yu J, Lu G, Zhao W, Miao C, Zou C, Wu J, Overcoming therapeutic failure in osteosarcoma via Apatinib-encapsulated hydrophobic poly(ester amide) nanoparticles, Biomater. Sci 8 (2020) 5888–5899. 10.1039/D0BM01296C. [PubMed: 33001086]

[34]. Lu X, Liu S, Han M, Yang X, Sun K, Wang H, Mu H, Du Y, Wang A, Ni L, Zhang C, Afatinib-loaded immunoliposomes functionalized with cetuximab: A novel strategy targeting the epidermal growth factor receptor for treatment of non-small-cell lung cancer, Int. J. Pharm 560 (2019) 126–135. 10.1016/j.ijpharm.2019.02.001. [PubMed: 30742982]

[35]. Gao W, Jia X, Wu J, Song Y, Yin J, Zhang M, Qiu N, Li X, Wu P, Qi X, Liu Z, Preparation and evaluation of folate-decorated human serum albumin nanoparticles for the targeted delivery of sorafenib to enhance antihepatocarcinoma efficacy, J. Drug Deliv. Sci. Technol 54 (2019) 101349. 10.1016/j.jddst.2019.101349.

[36]. Blair AB, Kim VM, Muth ST, Saung MT, Lokker N, Blouw B, Armstrong TD, Jaffee EM, Tsujikawa T, Coussens LM, He J, Burkhart RA, Wolfgang CL, Zheng L, Dissecting the Stromal Signaling and Regulation of Myeloid Cells and Memory Effector T Cells in Pancreatic Cancer, Clin. Cancer Res 25 (2019) 5351–5363. 10.1158/1078-0432.CCR-18-4192. [PubMed: 31186314]

[37]. Zinger A, Koren L, Adir O, Poley M, Alyan M, Yaari Z, Noor N, Krinsky N, Simon A, Gibori H, Krayem M, Mumblat Y, Kasten S, Ofir S, Fridman E, Milman N, Lübtow MM, Liba L, Shklover J, Shainsky-Roitman J, Binenbaum Y, Hershkovitz D, Gil Z, Dvir T, Luxenhofer R, Satchi-Fainaro R, Schroeder A, Collagenase Nanoparticles Enhance the Penetration of Drugs into Pancreatic Tumors, ACS Nano. 13 (2019) 11008–11021. 10.1021/acsnano.9b02395. [PubMed: 31503443]

[38]. Peng H, Shen J, Long X, Zhou X, Zhang J, Xu X, Huang T, Xu H, Sun S, Li C, Lei P, Wu H, Zhao J, Local Release of TGF-β Inhibitor Modulates Tumor-Associated Neutrophils and Enhances Pancreatic Cancer Response to Combined Irreversible Electroporation and Immunotherapy, Adv. Sci 9 (2022) 2105240. 10.1002/advs.202105240.

[39]. Chauhan VP, Martin JD, Liu H, Lacorre DA, Jain SR, Kozin SV, Stylianopoulos T, Mousa AS, Han X, Adstamongkonkul P, Popović Z, Huang P, Bawendi MG, Boucher Y, Jain RK, Angiotensin inhibition enhances drug delivery and potentiates chemotherapy by decompressing tumour blood vessels, Nat. Commun 4 (2013) 2516. 10.1038/ncomms3516. [PubMed: 24084631]

[40]. Aguilera KY, Huang H, Du W, Hagopian MM, Wang Z, Hinz S, Hwang TH, Wang H, Fleming JB, Castrillon DH, Ren X, Ding K, Brekken RA, Inhibition of Discoidin Domain Receptor 1 Reduces Collagen-mediated Tumorigenicity in Pancreatic Ductal Adenocarcinoma, Mol. Cancer Ther. 16 (2017) 2473–2485. 10.1158/1535-7163.MCT-16-0834. [PubMed: 28864681]

[41]. Massó-Vallés D, Jauset T, Serrano E, Sodir NM, Pedersen K, Affara NI, Whitfield JR, Beaulieu M-E, Evan GI, Elias L, Arribas J, Soucek L, Ibrutinib Exerts Potent Antifibrotic and Antitumor Activities in Mouse Models of Pancreatic Adenocarcinoma, Cancer Res. 75 (2015) 1675–1681. 10.1158/0008-5472.CAN-14-2852. [PubMed: 25878147]

[42]. Jain RK, Normalizing tumor vasculature with anti-angiogenic therapy: A new paradigm for combination therapy, Nat. Med 7 (2001) 987–989. 10.1038/nm0901-987. [PubMed: 11533692]

[43]. Carmeliet P, Jain RK, Principles and mechanisms of vessel normalization for cancer and other angiogenic diseases, Nat. Rev. Drug Discov 10 (2011) 417–427. 10.1038/nrd3455. [PubMed: 21629292]

[44]. Hosein AN, Brekken RA, Maitra A, Pancreatic cancer stroma: an update on therapeutic targeting strategies, Nat. Rev. Gastroenterol. Hepatol 17 (2020) 487–505. 10.1038/s41575-020-0300-1. [PubMed: 32393771]

[45]. Huang Y, Yuan J, Righi E, Kamoun WS, Ancukiewicz M, Nezivar J, Santosuosso M, Martin JD, Martin MR, Vianello F, Leblanc P, Munn LL, Huang P, Duda DG, Fukumura D, Jain RK, Poznansky MC, Vascular normalizing doses of antiangiogenic treatment reprogram the immunosuppressive tumor microenvironment and enhance immunotherapy, Proc. Natl. Acad. Sci 109 (2012) 17561–17566. 10.1073/pnas.1215397109. [PubMed: 23045683]

[46]. Batchelor TT, Gerstner ER, Emblem KE, Duda DG, Kalpathy-Cramer J, Snuderl M, Ancukiewicz M, Polaskova P, Pinho MC, Jennings D, Plotkin SR, Chi AS, Eichler AF, Dietrich J, Hochberg FH, Lu-Emerson C, Iafrate AJ, Ivy SP, Rosen BR, Loeffler JS, Wen PY, Sorensen AG, Jain RK, Improved tumor oxygenation and survival in glioblastoma patients who show increased blood perfusion after cediranib and chemoradiation, Proc. Natil. Acad.Sci 110 (2013) 19059–19064. 10.1073/pnas.1318022110.

[47]. Matsumoto S, Batra S, Saito K, Yasui H, Choudhuri R, Gadisetti C, Subramanian S, Devasahayam N, Munasinghe JP, Mitchell JB, Krishna MC, Antiangiogenic Agent Sunitinib Transiently Increases Tumor Oxygenation and Suppresses Cycling Hypoxia, Cancer Res. 71 (2011) 6350–6359. 10.1158/0008-5472.CAN-11-2025. [PubMed: 21878530]

[48]. Tsukita Y, Okazaki T, Ebihara S, Komatsu R, Nihei M, Kobayashi M, Hirano T, Sugiura H, Tamada T, Tanaka N, Sato Y, Yagita H, Ichinose M, Beneficial effects of sunitinib on tumor microenvironment and immunotherapy targeting death receptor5, OncoImmunology. 8 (2019) e1543526. 10.1080/2162402X.2018.1543526. [PubMed: 30713805]

Highlights:

- Nintedanib was successfully encapsulated within the pores of silicasomes, using a weak base remote loading approach.
- Improved pharmacokinetics and intratumor delivery of Nintedanib in an orthotopic KPC model.
- Nintedanib delivery associated with decreased collagen deposition and vascular density in the TME.
- Nintedanib increased $CD8^+$ T-cell recruitment, while significantly reducing Treg infiltration in PDAC tumor microenvironment.
- Nintedanib also increased PD-L1 expression, allowing αPD-1 to boost the immunotherapy response to Si-Ninte in PDAC.

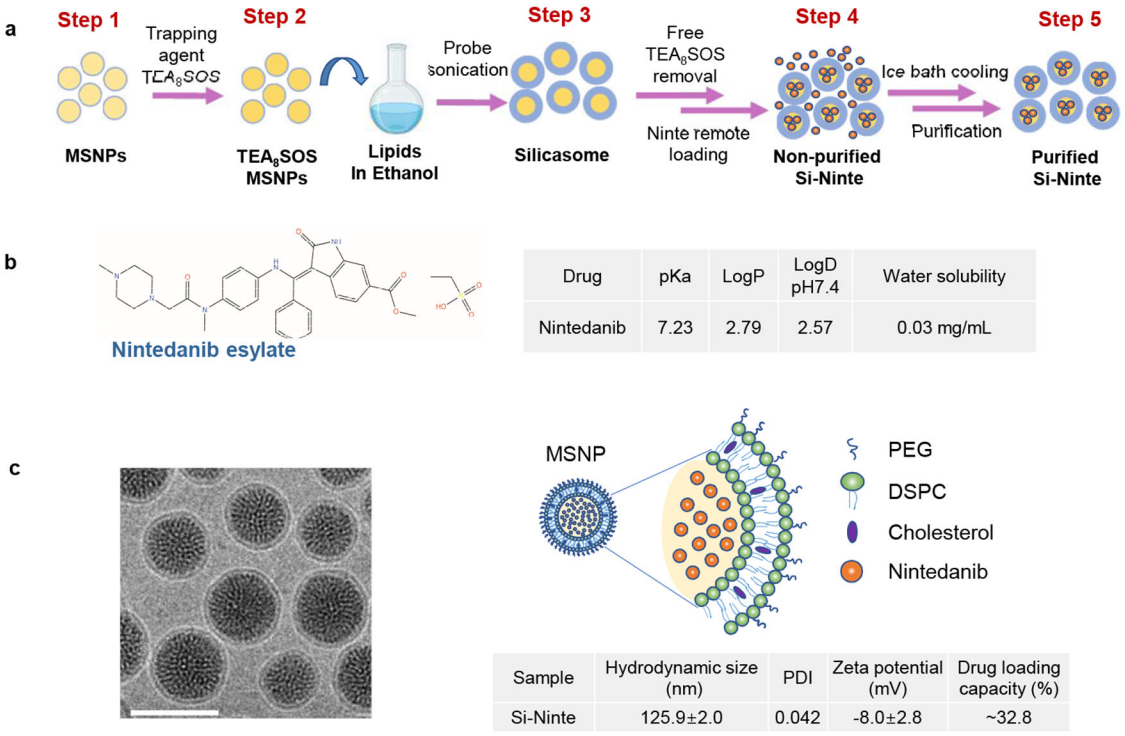

Fig. 1.

Silicasome nanocarrier development for Nintedanib delivery in PDAC. (a) Schematic to outline the synthesis steps for constructing the Silicasome-Nintedanib (Si-Ninte) carrier. (b) Schematic delineating the chemical structure and medicinal chemical properties of Nintedanib esylate, required for remote loading into mesoporous silica nanoparticles (MSNP) pores. Remote loading was accomplished by the use of soaking MSNPs in a trapping agent, TEA_8SOS. (c) CryoEM visualization and physicochemical properties of Si-Ninte (hydrodynamic size, polydispersity index (PDI), zeta potential, and drug loading capacity). Bar is 100 μm. The schematic depicts the supported lipid bilayer.

a

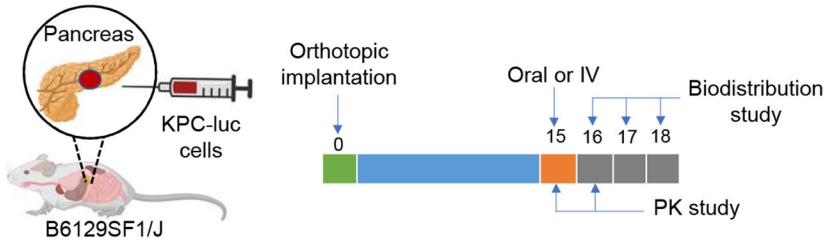

b

	Time					
PK study	10 min	30 min	1 h	3 h	9 h	24 h
Biodistribution study	24 h	48 h	72 h			

c

Sample	Size (nm)	PDI	Zeta potential (mV)
Si-Ninte-DIR	124.1±0.7	0.042	-7.36±0.7

d

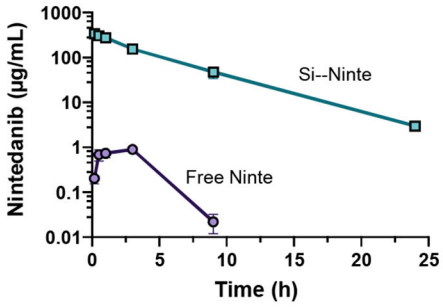

e

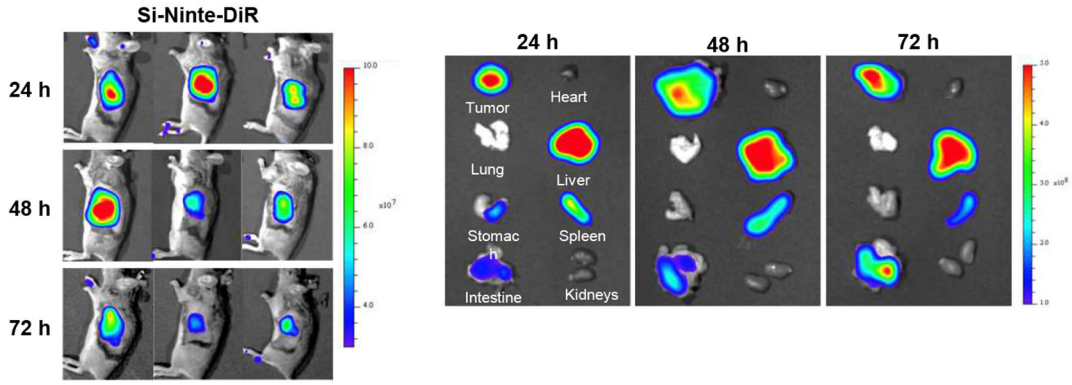

f

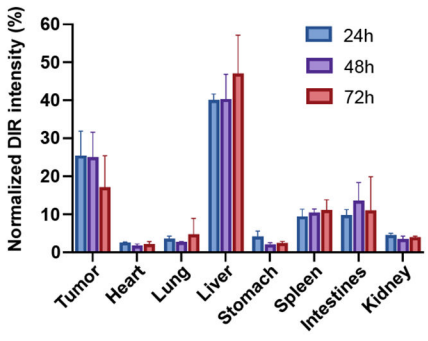

g

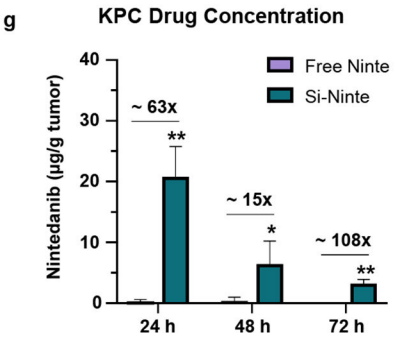

Fig. 2.

Improved pharmacokinetics and Nintedanib biodistribution in an orthotopic KPC model. (a and b) Experimental timeline for assessing blood levels and drug biodistribution by Si-Ninte compared to free drug in orthotopic tumor-bearing mice. The orthotopic implant involves injection of KPC-luc cells into the pancreas tail. Tumor-bearing animals were treated with single drug administration, involving oral gavage or IV injection of Si-Ninte to deliver 50 mg/kg Nintedanib (n = 3). (c) Physicochemical properties of DiR-labeled Si-Ninte. (d) Measurement of Nintedanib t plasma concentrations by HPLC, blood withdrawal on 6 occasions over 24 h. (e) In a separate experiment, using the same treatment regimen, *in vivo* DiR imaging was performed at 24, 48 and 72 hs (left-side panel). This was followed by animal sacrifice and *ex vivo* organ explantation and imaging (right-side panel). Fluorescence was expressed as radiant intensity. (f) Normalized fluorescence intensity of explanted organs. (g) The Nintedanib concentrations at the tumor sites were determined at different time points by HPLC. Data represent mean ± SEM. *$p < 0.05$, **$p < 0.01$.

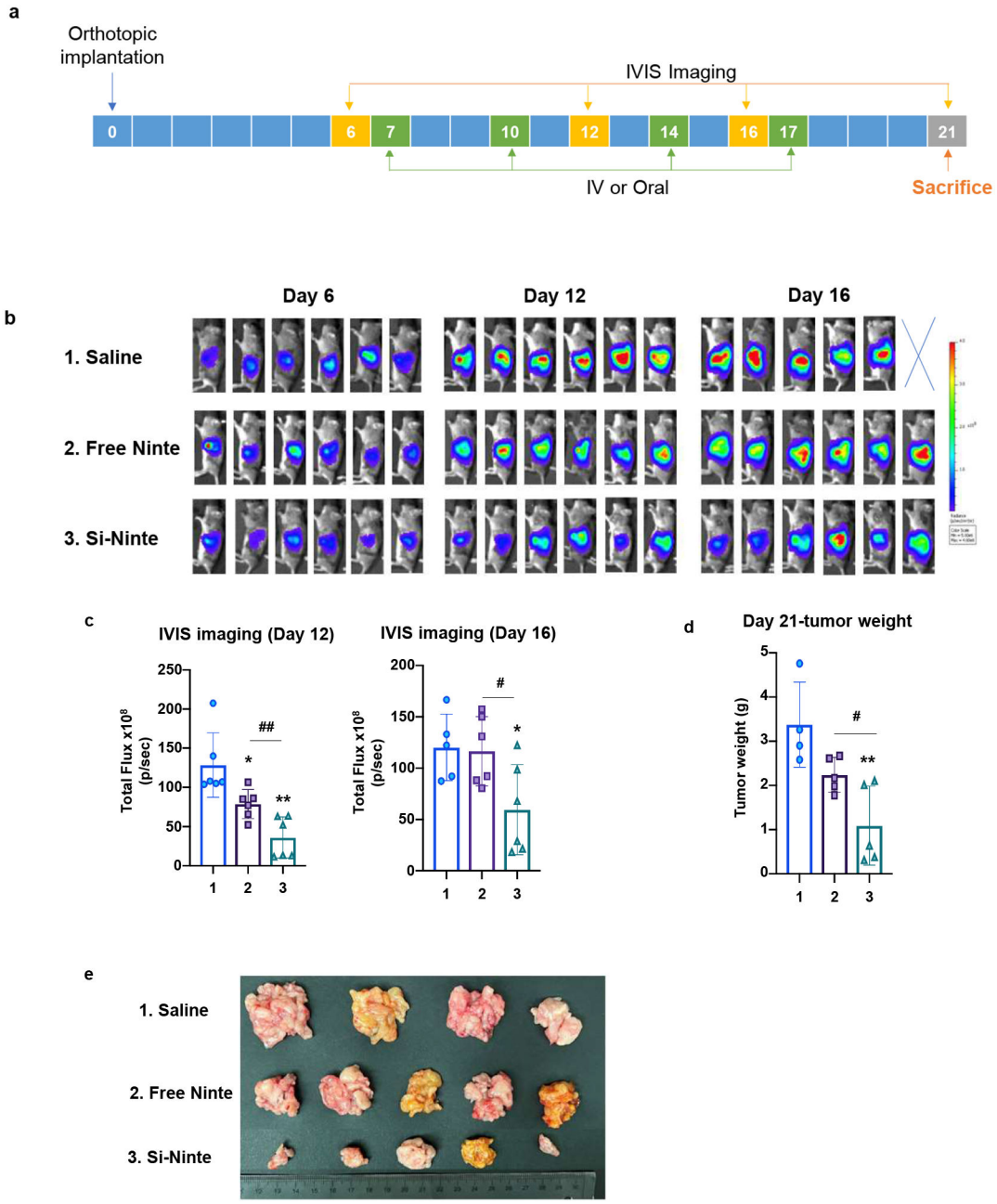

Fig. 3.

Nintedanib therapeutic impact on orthotopic tumor growth. (a) Experimental timeline to assess the therapeutic impact of oral-administered free Nintedanib vs. IV injected Si-Ninte in orthotopic KPC-luc tumor-bearing mice. (b) IVIS images tracking luminescence in KPC mice, following IV injection of saline, oral administration of free Nintedanib (50 mg/kg), or IV injection of Si-Ninte (10 mg/kg) twice a week for 2 weeks. (c) Average tumor bioluminescence intensity for each group (n=6) on days 12 and 16. Tumor growth inhibition by Si-Ninte was statistically significant ($p < 0.05$) compared to the saline control or free drug on day 16. (d) Comparison of average primary tumor weights in each group on day 21. (e) Photographic images of primary tumors, obtained on day 21. Body weight monitoring

did not show any significant differences among all groups (Fig. S3). Data represent mean ± SEM. *$p < 0.05$, **$p < 0.01$, $^{\#}p < 0.05$, $^{\#\#}p < 0.01$.

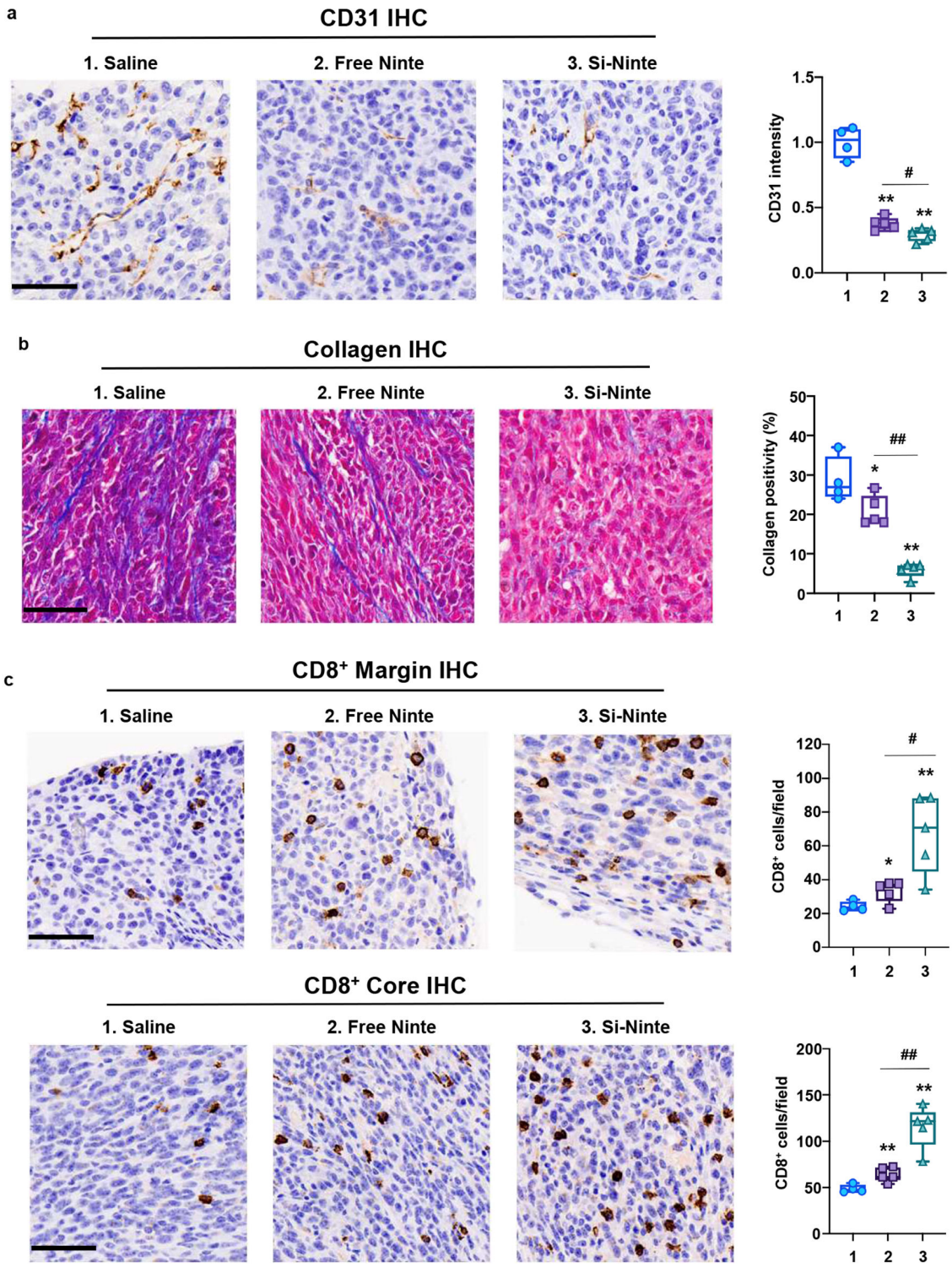

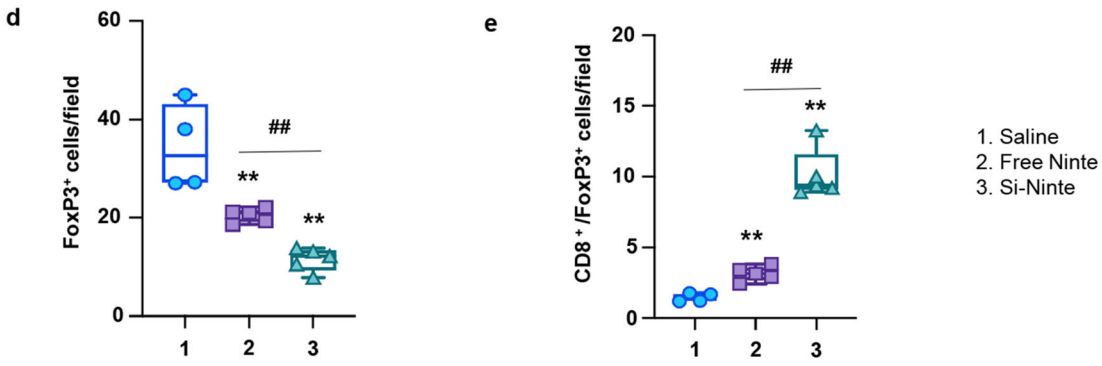

Fig. 4.

Immunohistochemistry (IHC) analysis of vasculature, collagen and immune infiltrates in orthotopic tumors. The harvested primary tumor tissues in Fig. 3 were used for IHC analysis of primary tumors from each treatment group, using random selection of 5 fields in each tumor for counting and averaging the positive staining events. Representative IHC images and quantification of: (a) CD31 staining intensity; (b) collagen staining intensity; (c) $CD8^+$ T-cell infiltrates and numbers in tumor margins and cores; (d) $FoxP3^+$ T-cell numbers in the tumor cores; (e) ratio of $CD8^+$ to $FoxP3^+$ T-cell numbers in the tumor cores. Representative staining panels for $FoxP3^+$ T-cell IHC analysis are shown in the supplementary results (Fig. S4). Bars are 50 μm. Data represent mean ± SEM. *$p < 0.05$, **$p < 0.01$, $^{\#}p < 0.05$, $^{\#\#}p < 0.01$.

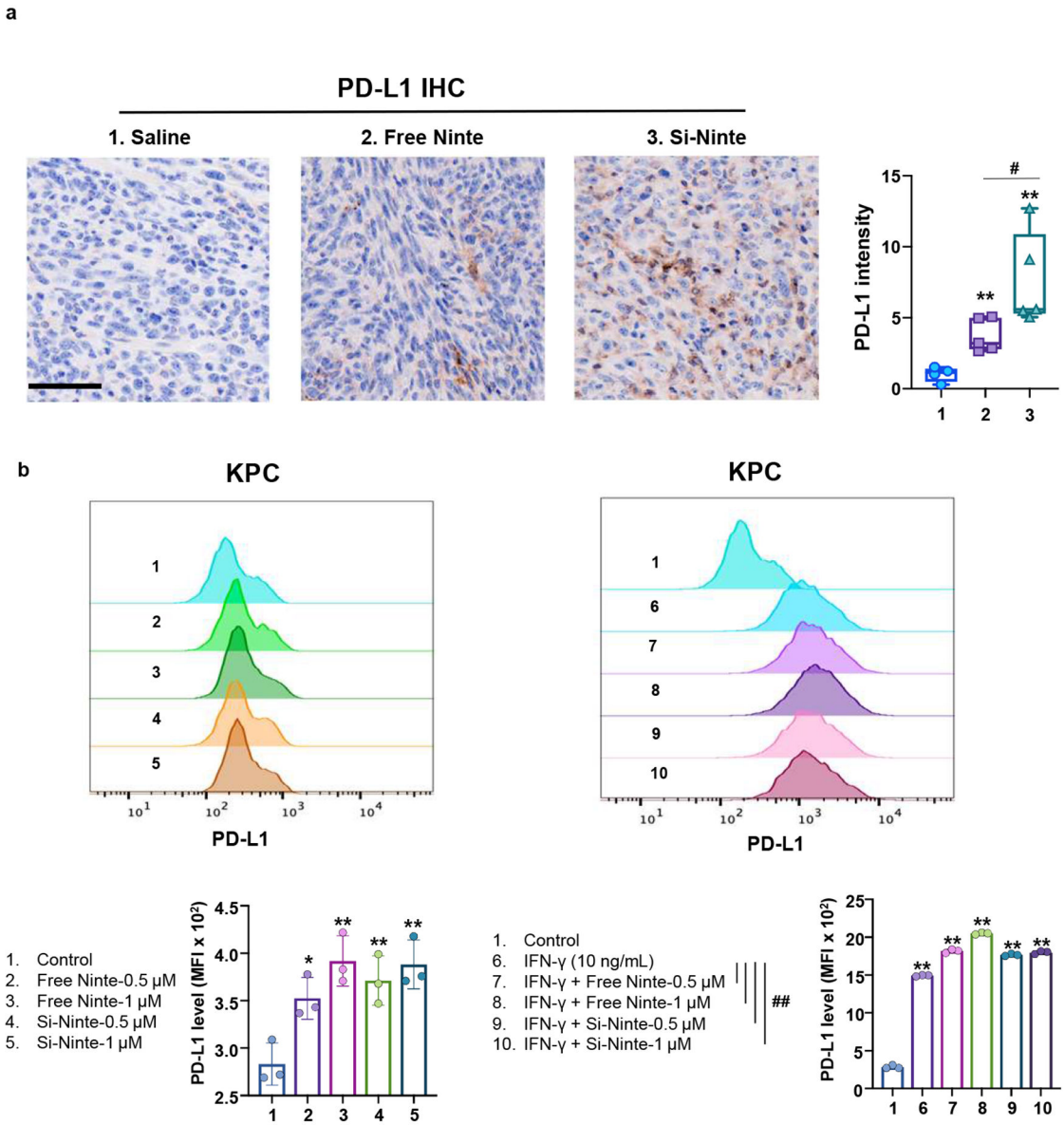

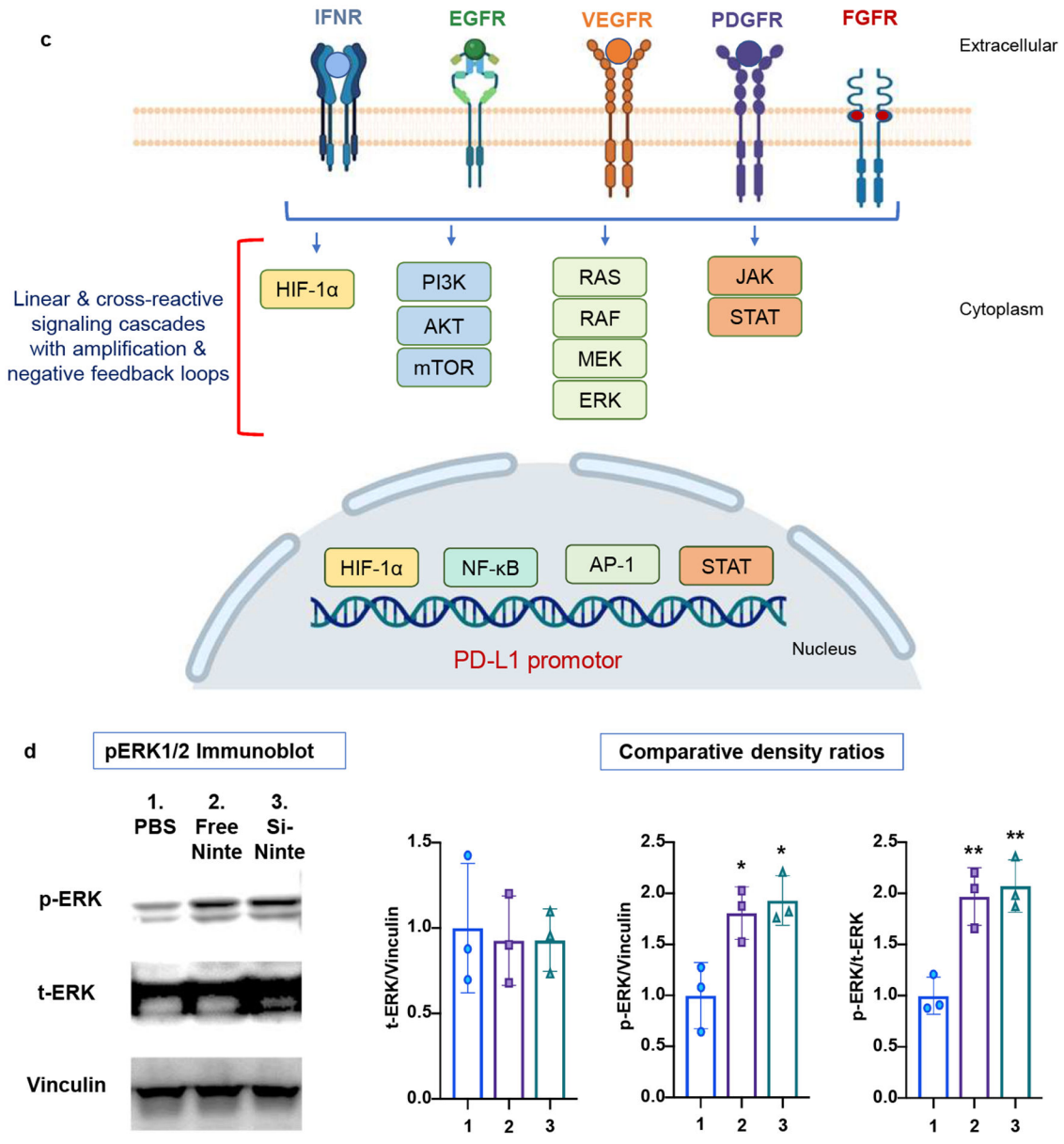

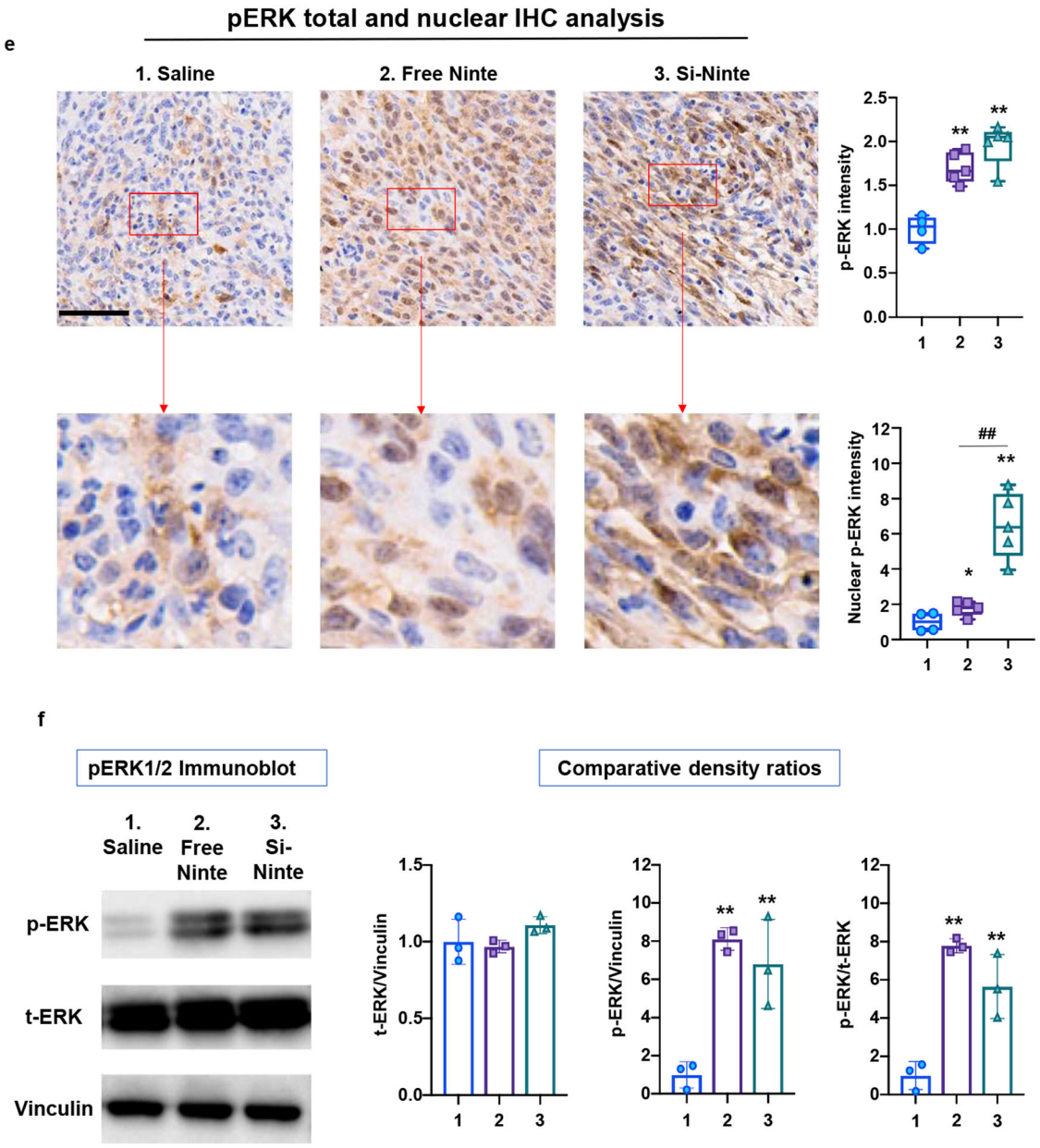

Fig. 5.

Nintedanib impact on PD-L1 expression *in vitro* and *in vivo*. (a) Representative IHC images, with quantification of PD-L1 intensity in tumors obtained from the orthotopic experiment in Fig. 3. (b) Flow cytometry analysis to quantify PD-L1 expression in the KPC cell line in response to different *in vitro* exposures. PD-L1 expression levels were evaluated by calculating MFI. (c) Schematic illustration of signaling pathways involved in transcriptional activation of the PD-L1 promotor in response to biological stimuli, including cytokines, hypoxia, toll-like receptor ligands and growth factors. The net result is determined by linear as well as interactive pathway connections, which depends on the contribution of each pathway in the TME. (d) Western blot analysis to access phosphorylation of ERK1/2 in KPC cells after treatment with free or encapsulated drug. Vinculin served as a stable-expressed

household protein for comparative analysis. (e, f) Tumor slices and protein extracts obtained from tumor tissues in Fig. 3 were used for IHC and western blot analyses. Panel e shows representative IHC images and quantification of pERK intensity in each group, while panel f shows the immunoblotting results and quantification of pERK1/2 expression. Bars are 50 μm. Data represent mean ± SEM. *$p < 0.05$, **$p < 0.01$, $^{\#}p < 0.05$, $^{\#\#}p < 0.01$. The study of STAT3 phosphorylation appears in Fig. S5.

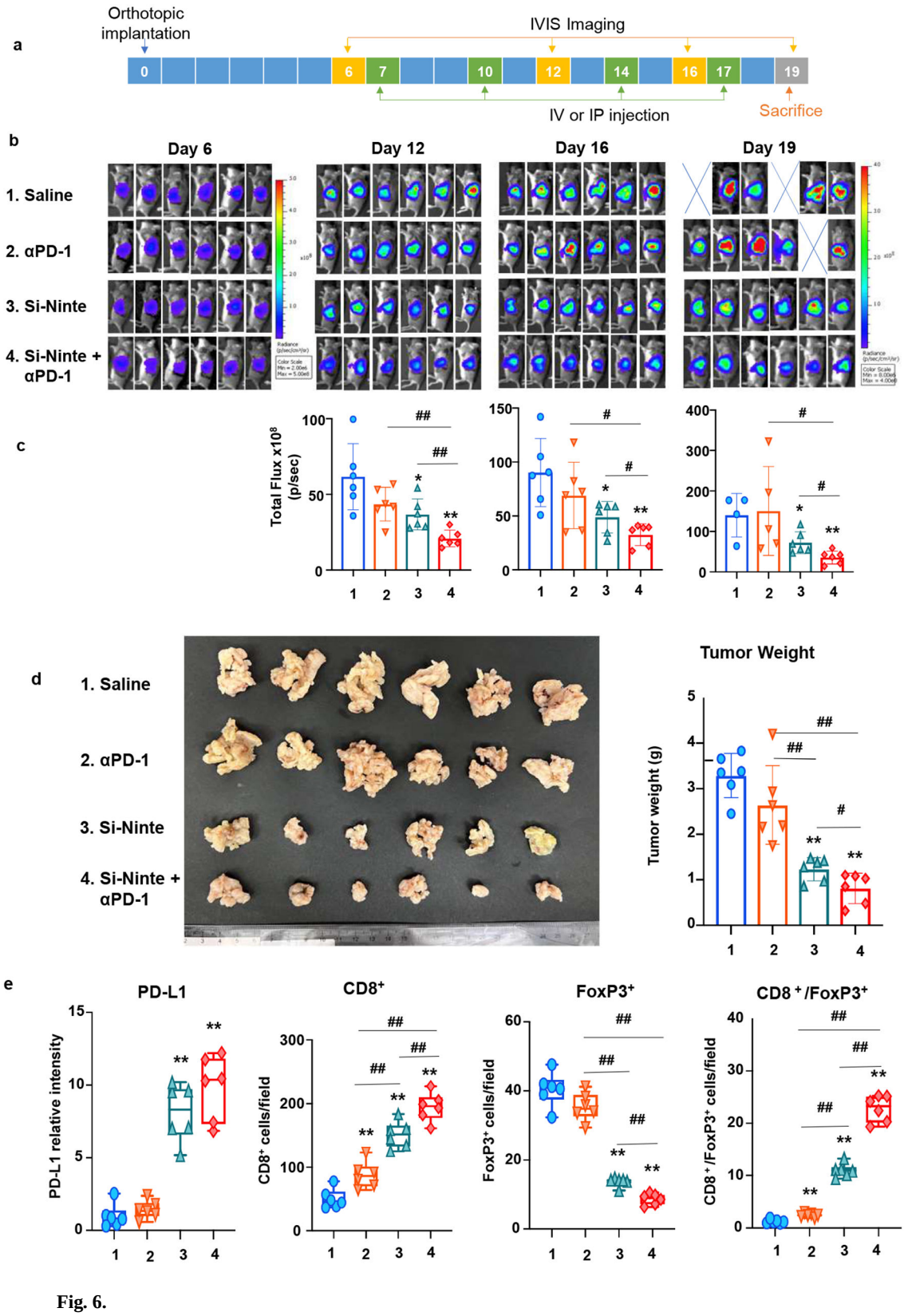

Fig. 6.

Anti-PD1 acts synergistically with Si-Ninte in immunotherapy for orthotopic KPC tumors. (a) Experimental timeline to assess the impact of combination therapy in orthotopic KPC-luc tumor-bearing mice (n = 6, per group). (b) IVIS images of tumor growth in animals receiving IV injection of saline, IP injection of αPD-1 (10 mg/kg), IV injection of Si-Ninte (10 mg/kg), or a combination of Si-Ninte IV plus αPD-1 IP, twice a week for 2 weeks. (c) Average tumor bioluminescence intensity for each group on days 12, 16 and 19. The inhibition of tumor growth by combination treatment is statistically significant compared to the saline control ($p < 0.01$) or single drug therapy ($p < 0.05$) on day 19. (d) Photographs and average primary tumor weights in each group on day 19. (e) IHC analysis to quantify PD-L1, $CD8^+$ and $FoxP3^+$ cell numbers in 6 primary tumors from each treatment group. 5 fields were randomly selected for analysis. Average cell numbers for each of the treatment groups are in the graphics. Representative staining panels for each IHC analysis are shown in the supplementary results (Fig. S6). Body weight monitoring every 2 days did not show any significant weight loss among all groups (Fig. S7). Data represent mean ± SEM. $^*p < 0.05$, $^{**}p < 0.01$, $^{\#}p < 0.05$, $^{\#\#}p < 0.01$.